European Journal of Medicinal Chemistry 316 (2026) 118947

Contents lists available at ScienceDirect

European Journal of Medicinal Chemistry

journal homepage: www.elsevier.com/locate/ejmech

Research paper

Structure-based design and synthesis of group A streptogramins that bind to the nascent peptide exit tunnel of the ribosome

Isabel J. Lee [a], Qi Li [a,b,*], Tushar Raskar [d], Jenna Pellegrino [d], Andrew K. Ecker [a,c], Sara Y. Howard [a], James S. Fraser [d], Ian B. Seiple [a,c,**]

[a] Department of Pharmaceutical Chemistry, Cardiovascular Research Institute, University of California – San Francisco, San Francisco, California, 94158, United States
[b] Small-Molecule Drug Research Center, Shanghai Institute of Materia Medica, Chinese Academy of Science, Shanghai, 201203, China
[c] Department of Chemistry, The Scripps Research Institute, La Jolla, California, 92307, United States
[d] Department of Bioengineering and Therapeutic Sciences, University of California – San Francisco, San Francisco, California, 94158, United States

ARTICLE INFO

Keywords:
Streptogramins
Antibacterial
Antibiotic resistance
Cryo-EM
Ribosome
Medicinal chemistry
TPSA

ABSTRACT

Natural products and their derivatives have long served as powerful tools for treating bacterial infections, but the rise of antibiotic resistance threatens their continued effectiveness. Targeted structural modification of existing classes of antibiotics is an effective strategy to overcome resistance and extend clinical utility. The development of group A streptogramins that overcome acetyltransferase resistance, a pervasive resistance mechanism to the class, is an example of successful implementation of this strategy. However, the synthetic chemistry to reach these new analogs was limited in its ability to access modifications at the C4 position on the scaffold, a promising modification site that produced the most potent streptogramin to date. Here, we report the development of a modified route to group A streptogramins that enables access to a broad diversity of functionality at C4. Using cryo-EM data to guide structural modifications, we synthesize several series of C4-modified group A streptogramins with sidechains designed to make binding contacts with the exit tunnel of the ribosome. We identify multiple analogs that are active against multidrug-resistant bacteria, including strains that are resistant to macrolides, β-lactams, vancomycin, and first-generation streptogramins. We structurally characterize the binding of two analogs to the bacterial ribosome, revealing new π-stacking interactions between the C4 sidechain and the non-canonical U1782-U2586 base pair. These findings demonstrate how structure-guided drug design can drive the development of next-generation antibiotics and increase the therapeutic potential of the streptogramin class.

1. Introduction

Streptogramin antibiotics are produced by *Streptomyces* spp. and are categorized into two classes: 23-membered macrocycles called group A streptogramins and 17-membered cyclic depsipeptides known as group B streptogramins [1]. Natural streptogramins have relatively low water solubility, preventing formulation for intravenous administration. The rise of vancomycin-resistant *Enterococcus faecium* (VREfm) infections in the 1990s, and the exceptional activity of streptogramin A/B combinations against VREfm, led to a surge of research aimed at optimizing these molecules for clinical use [1,2]. Dalfopristin/quinupristin (Synercid™), a combination of tertiary-amine containing streptogramins developed by Rhône-Poulenc, was approved by the FDA in 1999 for the treatment of VREfm bacteremia and complicated skin and skin structure infections caused by *Staphylococcus aureus* and *Streptococcus pyogenes* [3,4]. While effective, common side effects such as venous irritation and species-specific resistance have limited its use to cases where oxazolidinones or lipopeptides are not viable treatment options [5]. The first orally available streptogramin combination, flopristin-linopristin (NXL 103), had improved potency and met clinical endpoints in phase II clinical trials in 2011, but has not progressed further in the clinic due to company turnover and economic considerations [1].

Streptogramins inhibit bacterial protein synthesis by binding to adjacent sites in the bacterial ribosome: group A streptogramins bind to the peptidyl transferase center (PTC) to prevent peptide bond formation, while group B streptogramins bind to the adjacent nascent peptide exit

* Corresponding author. Department of Pharmaceutical Chemistry, Cardiovascular Research Institute, University of California – San Francisco, San Francisco, California, 94158, United States.
** Corresponding author. Department of Chemistry, The Scripps Research Institute, La Jolla, California, 92307, United States.
E-mail address: iseiple@scripps.edu (I.B. Seiple).

https://doi.org/10.1016/j.ejmech.2026.118947
Received 2 February 2026; Received in revised form 6 May 2026; Accepted 8 May 2026
Available online 9 May 2026

tunnel (NPET) to prevent polypeptide elongation and release [6]. Notably, group A streptogramins bind to the PTC first, resulting in structural rearrangement of the NPET to facilitate group B streptogramin binding [1,7]. Individually, both groups are bacteriostatic; however, when administered together, they exhibit synergistic activity that can be bactericidal against some species [1]. This synergy is explained at least in part by their cooperative binding, although it may not account for their pronounced synergistic effects in some species [7].

Growing antibiotic resistance has rendered many antibiotics, including streptogramins, less effective. One major resistance mechanism to group A streptogramins involves drug inactivation by virginiamycin *O*-acetyltransferase (Vat) enzymes, which acetylate the C18 alcohol to disrupt an important hydrogen bond interaction with the ribosomal RNA at G2505 and decrease their ability to bind to the ribosome [8]. Leveraging structural knowledge of Vat resistance and a modular synthesis platform of group A streptogramins, our group synthesized a preliminary library of analogs based on the natural product virginiamycin M2 (**VM2**) [9]. Two hit compounds (**SA1** and **SA2**, Fig. 1), which also incorporated the C16 fluorine found in flopristin (**1**), demonstrated potent activity against several bacteria harboring various forms of resistance including Vat resistance.

Examination of the cryo-EM structure of **SA1** and **VS1** bound to the *E. coli* ribosome reveals that the C4 allyl sidechain of **SA1** points toward **VS1**, nearly coming within van der Waals distance of the C7 aminobutyric acid sidechain (3.7 Å, Fig. 2A) [9]. This section of the NPET is also the binding site for the aromatic polyketide antibiotic tetracenomycin X (**2**), which participates in π-stacking with the non-canonical trans Watson-Crick/Watson-Crick geometry U1782-U2586 base pair (Fig. 2B) [10]. We hypothesized that an appropriately positioned aryl (or biaryl) group extending from C4 on group A streptogramins would participate in π-stacking with U1782-U2586, mimicking tetracenomycin's productive binding in this region. A similar strategy has been employed in ketolide antibiotics, such as telithromycin and solithromycin, wherein addition of an aryl-containing sidechain facilitates π-stacking interactions with the A752-U2609 base pair (see SI Figure S1), resulting in substantially enhanced potency over macrolides such as erythromycin [11–13].

Since further extension of C4 would preclude binding of group B streptogramins, this approach would effectively replace the group A + B streptogramin antibiotic combination with a single, structurally expanded group A streptogramin antibiotic. While this would implicitly result in a loss of synergy, it would have the notable advantage of circumventing group B streptogramin resistance mechanisms. For example, this extension of streptogramin A should not be affected by Erm-mediated methylation of A2058 (Fig. 2B), which causes resistance to macrolides, lincosamides, and group B streptogramins like **VS1** (MLS_B phenotype), or by mutations of A2058 and A2059 [14]. Moreover, C4-modified group A streptogramins would not be substrates for Vgb lyases, which deactivate group B streptogramins by ring cleavage [15]. Thus, this approach may completely avoid several resistance mechanisms that target the B component of streptogramin A + B combinations. Despite these potential advantages, it was unclear whether group A streptogramins with extended binding footprints could reach the same level of potency as group A + B streptogramin combinations. Herein, we report two preliminary series of analogs designed to test this general approach.

2. Results and discussion

2.1. Synthesis of an amide linker series

Our previous syntheses of group A streptogramins comprised the assembly of several building blocks into two halves of approximately equal complexity, which could then be coupled, macrocyclized, and deprotected to provide final antibiotic candidates [9,16–18]. In principle, each of the building blocks could be varied, enabling modular

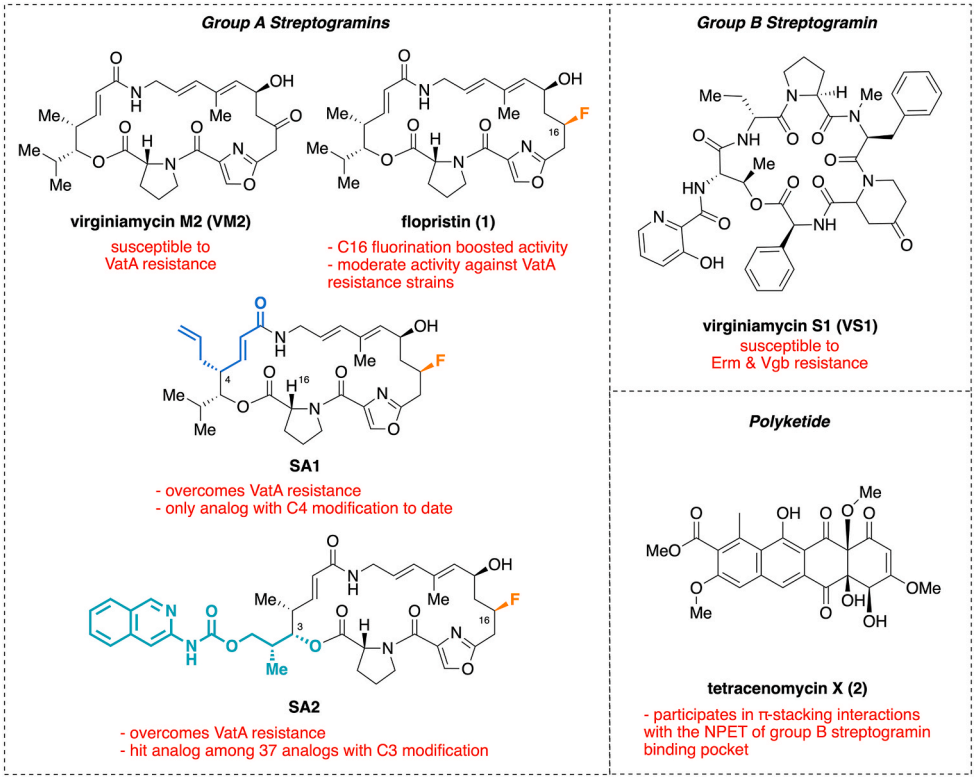

Fig. 1. Selected natural and synthetic group A and group B streptogramins, along with polyketide antibiotic tetracenomycin X (**TcmX**). Modifications of parent scaffold are highlighted: C16 fluorination of flopristin (**1**), **SA1**, and **SA2** are highlighted in orange, C4-modified sidechain of **SA1** is highlighted in blue, and C3-modified sidechain of **SA2** is highlighted in teal.

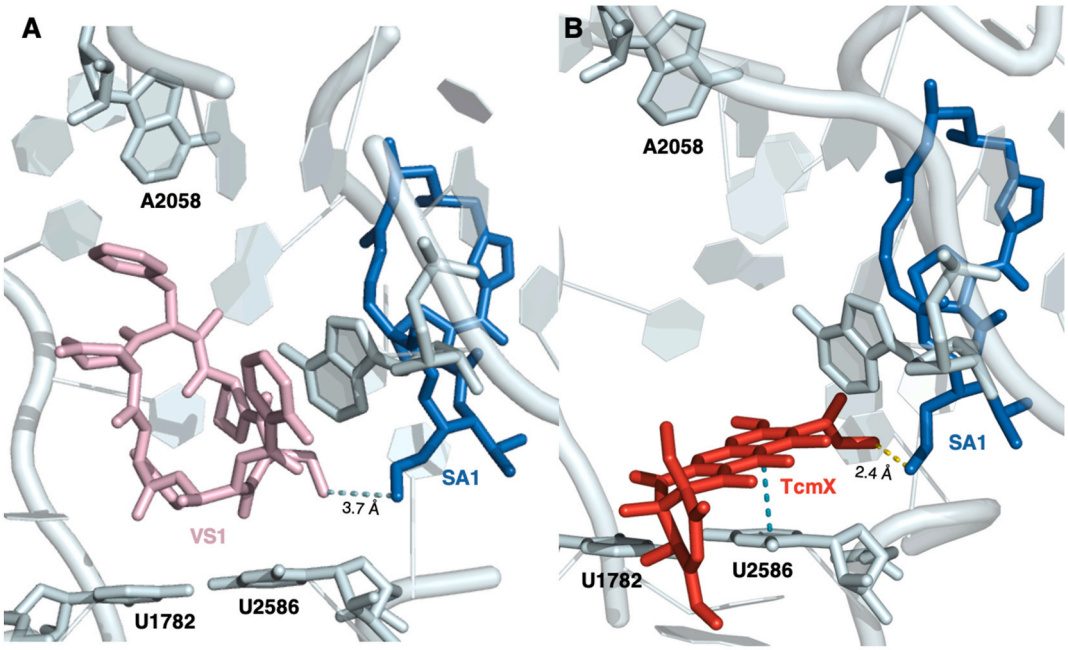

Fig. 2. A. Cryo-EM structure of ribosome-bound **SA1** (blue) and **VS1** (pink) (PDB code 6WYV) [9] reveals C4 sidechain pointing towards the binding pocket of VS1. **B.** Overlay of cryo-EM structures of ribosome-bound **SA1** (blue) (PDB code 6PC6) [9] and **TcmX** (red) (PDB code 6Y69) [10]. **TcmX** makes π-stacking interactions (blue dashed line) with U1782-U2586, and **TcmX** is 2.4 Å away (yellow dashed line) from the C4 sidechain of **SA1**.

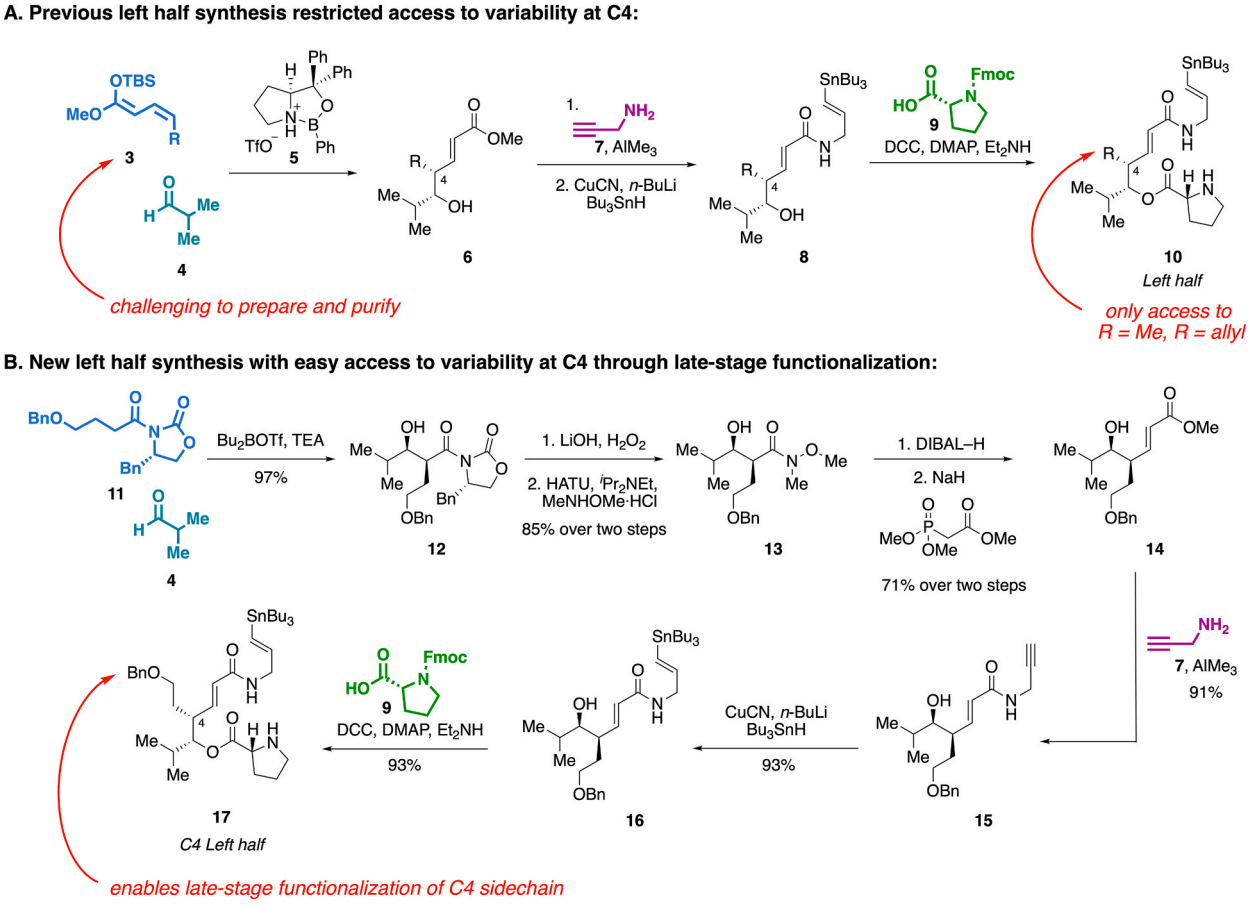

Scheme 1. A. Previously reported left half synthesis with limited variability at C4 position. **B.** Updated left half synthesis with access to variability at C4 position through late-stage functionalization. Bn = benzyl, Bu = butyl, DCC = dicyclohexylcarbodiimide, dba = dibenzylideneacetone, DMAP = 4-dimethylaminopyridine, Fmoc = 9-fluorenylmethoxycarbonyl, HATU = 1-[Bis(dimethylamino)methylene]-1H-1,2,3-triazolo[4,5-*b*]pyridinium-3-oxidhexafluorophosphate, TBS = *tert*-butyldimethylsilyl, TEA = triethylamine, TfO = trifluoromethanesulfonate.

replacement of functionality in the final products. In practice, however, the synthesis was not always compatible with additional functionality included in modified building blocks. For example, the vinylogous Mukaiyama aldol reaction that initiated the synthesis of left half **10** required the preparation of unstable silyl ketene acetals such as **3**, which were purified by distillation and had limited variability (Scheme 1A). This restricted the ability to modify positions on this building block, resulting in access to only two C4-modified analogs in our previous report [9]. To further explore this portion of the molecule and to test our hypothesis of group B streptogramin replacement, we designed a new synthesis of the left half of group A streptogramins that permits expanded functionalization at C4 (Scheme 1B).

We chose to include an alcohol as a functional handle for late-stage derivatization, shielding it as a benzyl ether throughout the synthesis. Our route to the C4-modified left half **17** commenced with an Evans aldol reaction between isobutyraldehyde (**4**) and oxazolidinone **11** (available in 3 steps from 1,4-butanediol) to provide aldol product **12** in 97% as a single diastereomer [19]. Hydrolysis of the Evans auxiliary yielded the corresponding carboxylic acid, which was converted to Weinreb amide **13** in 85% yield (2 steps). Reduction with diisobutylaluminum hydride (DIBAL) furnished the crude aldehyde, which was subjected to a Horner-Wadsworth-Emmons (HWE) olefination to afford ester **14** in 71% yield (2 steps) as a single diastereomer [20].

Subsequent transformations followed the previously established synthesis of **VM2** left half [9,16]. Amidation of ester **14** with propargylamine **7** in the presence of trimethylaluminum followed by hydrostannylation of the resulting terminal alkyne in **15** afforded vinyl stannane **16** in 85% yield over two steps. Final esterification of vinyl stannane **16** with Fmoc-protected D-proline **9** using DCC and catalytic DMAP, followed by addition of diethylamine, afforded the complete C4-modified left half **17** in 93% yield. This eight-step sequence proceeded in 46% overall yield from building blocks **4** and **11**, and provided decagrams of **17**.

The previously developed route to the right half was designed to access group A streptogramins with a ketone at the C16 position, such as the natural product **VM2** [16,17]. This enabled the synthesis of over 50 C16-keto analogs. Inspired by flopristin (**1**), which incorporated a fluorine at C16 and displayed enhanced activity over **VM2**, three

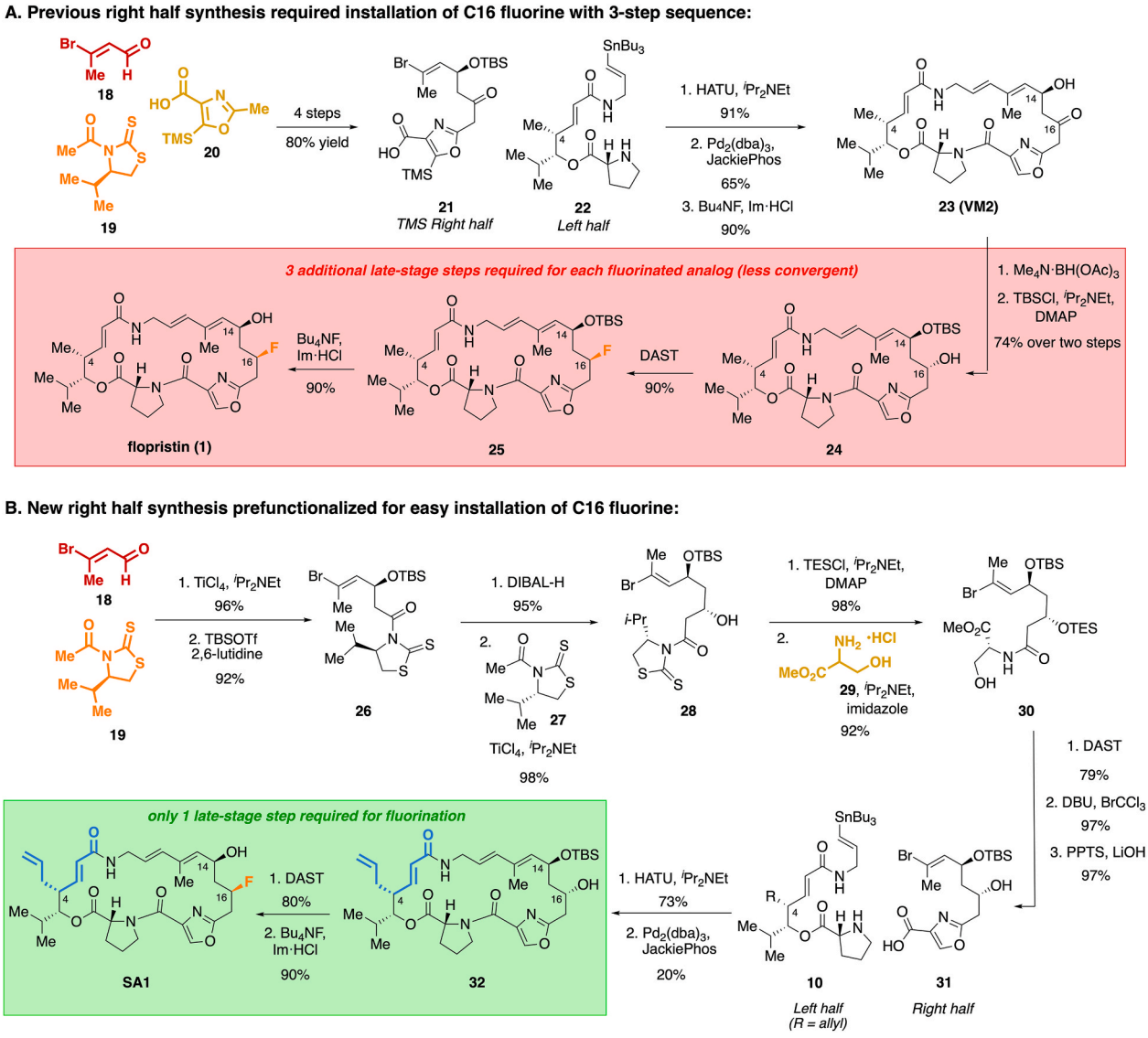

Scheme 2. A. Previously reported right half synthesis required three late-stage step sequence to C16 fluorination. **B.** Updated right half synthesis prefunctionalized for C16 fluorination in one step. Bu = butyl, DBU = 1,8-diazabicyclo[5.4.0]undec-7-ene, dba = dibenzylideneacetone, DMAP = 4-dimethylaminopyridine, HATU = 1-[Bis(dimethylamino)methylene]-1H-1,2,3-triazolo[4,5-*b*]pyridinium-3-oxidhexafluorophosphate, Im = imidazole, TBS = *tert*-butyldimethylsilyl, TEA = triethylamine, TES = triethylsilyl, TfO = trifluoromethanesulfonate, TMS = trimethylsilyl.

analogs were fluorinated using a late-stage three-step sequence (Scheme 2A). These fluorinated analogs had substantially improved activity compared to their non-fluorinated versions [9]. However, the requirement for three additional steps at the final stages of the synthesis, including a sensitive diastereoselective reduction and reprotection of the C14 alcohol which would later be deprotected again, inherently limited the number of C16-fluorinated analogs that could be generated. Specifically, for each modified left half that was synthesized, 7 steps were required to reach final fluorinated analogs. This became particularly costly with left halves that were challenging to acquire at large scale.

Since C16-fluorinated derivatives exhibited consistently higher activity in all strains, we sought to design a synthesis of a prefunctionalized right half that would reduce the number of steps required to install the fluorine at the late stage of the synthesis, thus increasing convergency at the cost of a longer right half synthesis. While all attempts to include the C16 fluorine on the right half prior to coupling failed, we were able to develop a route to right half **31**, which contains an alcohol that can be deoxyfluorinated in a single penultimate step. This design reduced the late-stage synthetic burden, requiring only 3 steps to reach final compounds after the coupling of the halves. A first iteration of this strategy was employed in the synthesis of **SA1**, necessitated by the low material throughput due to a poor macrocyclization yield (26%) for the C4-allyl series, which precluded four additional steps at a late stage [9]. Here, we discuss this adapted right-half route in detail and apply it to the synthesis of two series of antibiotic candidates with C16 fluorination (Scheme 2B).

Our synthesis of right half **31** commenced with the aldol coupling of (*E*)-3-bromobut-2-enal (**18**, available in 3 steps from crotyl alcohol) and acetyl thiazolidinethione **19** (2 steps from (R)-valinol) to afford aldol product in 96% yield as a single diastereomer [21–24]. Subsequent protection of the secondary alcohol with *tert*-butyldimethylsilyl trifluoromethanesulfonate (TBSOTf) afforded *tert*-butyldimethylsilyl (TBS)-protected alcohol **26**. Reduction of TBS-protected aldol product **26** with DIBAL furnished aldehyde in 95% yield, which was subjected to another aldol coupling with acetyl thiazolidinethione **27** (2-steps from (S)-valinol) to afford aldol product **28** in 98% yield as a single diastereomer. Protection of the newly formed secondary alcohol using triethylsilylchloride (TESCl), *N*,*N*-diisopropylethylamine (DIPEA), and catalytic DMAP afforded triethylsilyl (TES) ether in 98% yield. Displacement of the thiazolidinethione auxiliary with L-serine methyl ester hydrochloride **29** furnished oxazole precursor **30** in 92% yield, which was treated with diethylaminosulfur trifluoride (DAST) and DBU and bromotrichloromethane to afford the cyclized oxazole product in 77% yield over two steps [25]. Global deprotection with pyridinium *p*-toluenesulfonate (PPTS) and lithium hydroxide provided the complete right half **31** in 97% yield. The nine-step sequence proceeded in 54% yield from building blocks **18** and **19**, providing decagrams of **31**. This was then carried forward to the final compound **SA1** in only four steps. Similar to the C16-keto series, macrocyclization proceeded in low yield (20%), but the higher degree of convergency enabled access to C4-allyl, C16-fluoro series in sufficient quantities to enable *in vitro* and *in vivo* evaluations efficacy [9]. This route to the right half also enabled the synthesis of all of the analogs discussed herein, avoiding costly late-stage fluorination.

With an abundant supply of right half **31** and a highly convergent route in hand, we initiated the synthesis of other C4-modified, C16-fluorinated group A streptogramins. Coupling of left half **17** with right half **31** using HATU afforded the full linear precursor in 86% yield (Scheme 3) [9]. Macrocyclization via Stille coupling in the presence of tris(dibenzylideneacetone)dipalladium(0) ($Pd_2(dba)_3$) yielded macrocycle **33** in 68% yield [16]. The C16 fluorine was then installed with DAST, and benzyl deprotection afforded alcohol **34** in 65% yield (2 steps). Sequential oxidation of **34** with Parikh-Doering and Pinnick conditions provided carboxylic acid **35** in 86% yield over two steps [26–28]. Coupling of **35** to 2-azidoethylamine **36** using HATU afforded diversifiable intermediate **37**. The route to intermediate **37** proceeded in 18% overall yield from building blocks **4** and **11** (15 steps) or 11% overall yield from building blocks **18** and **19** (16 steps). We were able to functionalize the azide handle by allowing it to react with various aryl alkynes in the presence of copper (II) sulfate and sodium ascorbate [29]. Final desilylation afforded novel C4-modified group A streptogramin analogs **38** bearing a variety of aryltriazole sidechains (Fig. 3A).

We evaluated a select number of this series for their ability to inhibit bacterial protein synthesis *in vitro* in an *E. coli* ribosome-based transcription-coupled translation assay. Compounds **38a-e** potently inhibited translation at 10 μM, demonstrating the on-target activity of the analogs (Fig. 3B). We then acquired cryo-EM data to 2.4-Å resolution that resolved **38d** revealing the predicted π-stacking of the triazole-pyridyl group (in blue) with U2586 and U1782, showing the importance of the aryl rings at the C4 extension (Fig. 3C). We also acquired cryo-EM data to 1.9-Å resolution of **38a** (PDB code 8E30) which revealed identical positioning of the macrocycle but had two densities for the aminomethyltriazole, one of which was engaging in π-stacking interactions [31]. This suggests that the presence of an aryl group on the triazole assists in positioning of the sidechain. Despite the favorable binding and *in vitro* inhibitory activity, only a few of these analogs were able to inhibit the growth of bacteria at high concentrations (32-64 μg mL^{-1}, Fig. 3A, SI Figures S2 and S3).

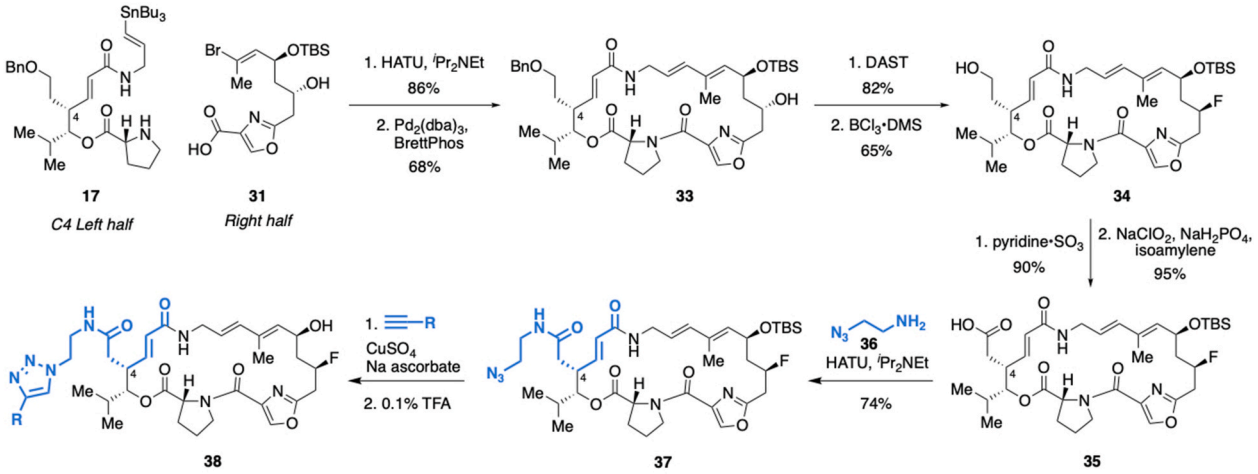

Scheme 3. Synthesis of C4-modified group A streptogramin analogs. Access to novel analogs **38** with different R substituents. Bn = benzyl, dba = dibenzylideneacetone, DMS = dimethyl sulfide, HATU = 1-[Bis(dimethylamino)methylene]-1H-1,2,3-triazolo[4,5-*b*]pyridinium-3-oxidhexafluorophosphate, TBS = *tert*-butyldimethylsilyl.

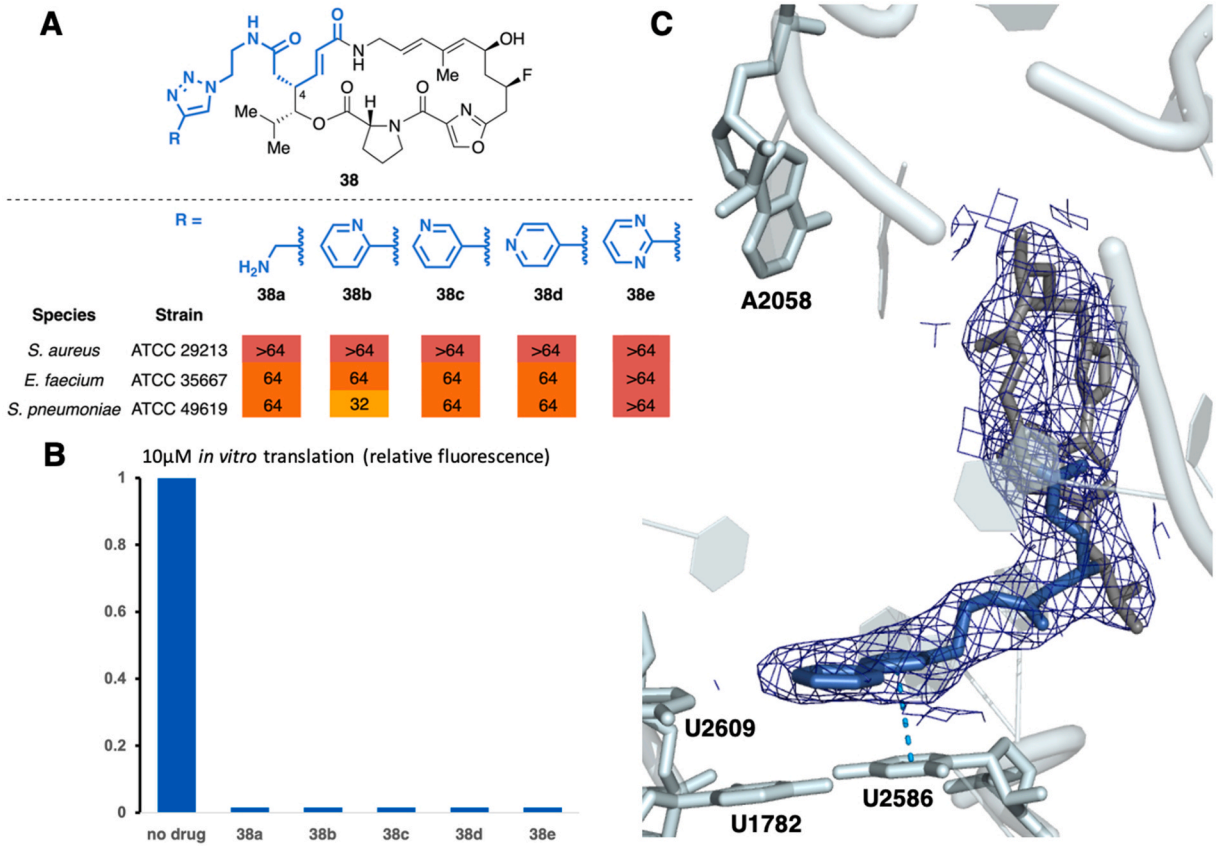

Fig. 3. **A.** MIC values (μg mL^{-1}) of selected analogs **38** against selected strains. Each MIC was obtained in triplicate. **B.** The graph displays *in vitro* translation of GFP that occurs in the presence of 10 μM of each analog (relative to dimethylsulfoxide (DMSO)). **C.** Cryo-EM structure built into a 2.4-Å resolution Coulomb potential density map for ribosomes bound to **38d** (PDB code 8E36) [30]. **38d** is making a π-stacking interaction (blue dashed line) with U2586.

The discrepancy between the *in vitro* and *in vivo* activities of these analogs suggests that factors affecting cellular accumulation may be hindering the ability of analogs to reach and engage the ribosome within bacterial cells [32]. One key barrier that limits cellular entry is membrane permeability. Although many antibiotics violate Lipinski's Rule of Five – given the distinct nature of bacterial versus eukaryotic cellular envelopes – properties such as high polar surface area (PSA) can still adversely impact permeability and cellular entry [32,33]. Efflux is another major determinant of intracellular drug concentrations and a common antibiotic resistance mechanism [34].

To directly assess the contributions of these factors, we evaluated compounds **38a-e** in efflux-deficient and permeability-compromised *E. coli* (see SI Figure S3). In both strain types, we saw a 2- to 8- fold improvement in potency compared to wild-type cells (>64 vs 8-32 μg mL^{-1}). While Gram-negative bacteria possess an outer membrane and more extensive multidrug efflux pumps compared to Gram-positive bacteria, the observed increase in activity in both efflux-deficient and permeability mutants of *E. coli* suggests that both processes contribute to limited compound efficacy [35]. These results suggest that both reduced permeability and active efflux reduce intracellular accumulation of these analogs, thereby diminishing their antibacterial activity.

Guided by these observations, we considered how structural features of these analogs might influence accumulation. We hypothesized that the secondary amide connecting the alkyl-triazole sidechain to the macrocycle may be increasing the exposed polar surface area (EPSA) of the analogs, which could impact cellular uptake. We noted that EPSA alone was unlikely to fully account for the observed loss of activity, as efflux could also be a factor. However, reducing EPSA and improving permeability could improve intracellular accumulation and regain some cellular activity. Unfortunately, parallel artificial membrane permeability assays (PAMPA) are known to be poor predictors of bacterial cell accumulation, which have different cellular envelopes than eukaryotic cells and robust mechanisms for efflux of small molecules [36]. Therefore, predicting bacterial permeability and accumulation often necessitates alternative approaches, including considering PSA of the molecules.

2.2. Using TPSA for analog design

Calculated PSA is often used as a predictive metric for cell permeability, where higher PSA correlates with poor cell membrane permeability. Two complementary measures of molecular polarity are topological polar surface area (TPSA) and EPSA. TPSA is a 2D, topology-based estimate of surface area contributed by the polar atoms and their attached protons on the molecule [37,38]. In contrast, EPSA is an experimentally derived value intended to reflect a compound's effective polarity in solution, capturing conformational shielding and intramolecular interactions that can modulate how much polar surface area is exposed [39]. EPSA can be a more informative descriptor of effective polarity because it reflects (either experimentally or via conformationally informed computation) how 3D structure and intramolecular shielding modulate the polar surface area that is exposed in solution. However, for large, conformationally dynamic macrocycles, EPSA is not always straightforward to obtain or interpret. Robust conformational sampling can be computationally demanding and experimentally determined EPSA values (by supercritical fluid chromatography (SFC)) may be sensitive to assay conditions and may not fully reflect the solution ensemble most relevant to bacterial entry [40]. In this series, because the core macrocycle is conserved and variation is confined to the sidechains, TPSA provides a practical comparator for identifying

trends in polarity and a potential working TPSA window associated with whole-cell activity in these streptogramin analogs.

We calculated the TPSA values, computed by the descriptors module in Molecular Operative Environment, for hit compounds **SA1** and **SA2,** as well as for analog **38d** (Fig. 4). **SA1** and **SA2,** which exhibit antibacterial activity and thus are assumed to efficiently accumulate in bacteria, have calculated TPSA values of 122 $Å^2$ and 173 $Å^2$, respectively. In contrast, analog **38d**, which lacks cellular activity, has a higher TPSA of 195 $Å^2$. These results suggest that there may be a TPSA threshold of <195 $Å^2$ in which cell penetration is favorable.

We also calculated TPSA values for analogs with isosteric replacements for the amide group in the C4 linker. *N*-methylated amide and ester substitutions have shown to be the simplest and most effective methods in reducing EPSA of amide-containing compounds, reducing EPSA by around 12-15 $Å^2$ [39]. Given that the initial C4 analog **SA1** —bearing an allyl group— showed enhanced activity, replacing the amide with a full carbon chain could also improve both permeability and activity. Of all the different amide bioisostere replacements, we found that replacing the amide with an alkyl chain reduced TPSA the most (to 166 $Å^2$ for a 4-pyridyltriazole sidechain), placing it within the TPSA range of the two active hit compounds **SA1** and **SA2**. With that in mind, we designed a synthesis of a new series of analogs featuring alkyl chain linkers of varying lengths.

2.3. Synthesis of an alkyl linker series

Our synthesis of the alkyl linker series followed a strategy analogous to that of the amide linker series, with specific adjustments made to accommodate the azide-containing sidechain (Scheme 4A). The synthesis commenced with an Evans aldol addition between oxazolidinone **39** and isobutyraldehyde **4**. $TiCl_4$, DIPEA, and NMP were used in place of Bu_2BOTf, as $TiCl_4$ offers a cost-effective alternative without compromising yield (85%) [41]. Reduction of the resulting Weinreb amide **41** with DIBAL proved to be ineffective for aldehyde formation. Even with increased loading of DIBAL, extended reaction times, and alternative solvent systems, there was minimal conversion to aldehyde. Lithium aluminum hydride ($LiAlH_4$), a stronger reductant, led to partial conversion to aldehyde and some over-reduction to the alcohol. Unreacted Weinreb amide **41** could be recovered during purification and resubjected to $LiAlH_4$ reduction, which increased aldehyde yields from 67% to 80%.

Amidation of ester **42** with propargylamine (**7**) in the presence of trimethylaluminum provided terminal alkyne in **43**. Hydrostannylation of this alkyne initially employed copper catalysis, however this led to a primary amine as a major byproduct, likely due to copper(I)-mediated reduction of the azide function. To preserve the azide, we adopted the palladium-catalyzed protocol developed by Darwish et al. utilizing $Pd_2(dba)_3$, Cy_3PHBF_4, and DIPEA, which enabled regioselective formation of the desired *E*-vinyl stannane **44** without azide reduction [42]. Efforts to purify vinyl stannane **44** through column chromatography were complicated by its instability on silica [43,44], but the addition of triethylamine to the solvent system mitigated the decomposition and improved yields from 32% to 59%.

The coupling of left half **45** with right half **31** using HATU resulted in modest yield (47%), but substitution of HATU with PyAOP increased the yield to 59%. Stille macrocyclization with $Pd_2(dba)_3$ in the presence of BrettPhos provided macrocycle **46** in 58% yield [16,45]. Deoxyfluorination at C16 provided fluorinated macrocycle **47** in 80% yield. Importantly, the reduced step count in these late stages of the redesigned synthesis enabled the synthesis of gram quantities of **47** from similar amounts of left half **45**, obviating the need for a decagram synthesis of this half. The 5-carbon linker route to **47** proceeded in 6% overall yield from building blocks **4** and **39** (11 steps).

Synthesis of the shorter 4-carbon linker-containing left half **52** followed the same route as the 5-carbon linker left half **45**, but starting with Evans addition using oxazolidinone **49**, which was readily obtained in one step from 6-azidohexanoic acid (Scheme 4B). Left half **52** was carried forward to diversifiable macrocycle **54**. The 4-carbon linker route to **54** proceeded in 5% overall yield from building blocks **4** and **49** (11 steps).

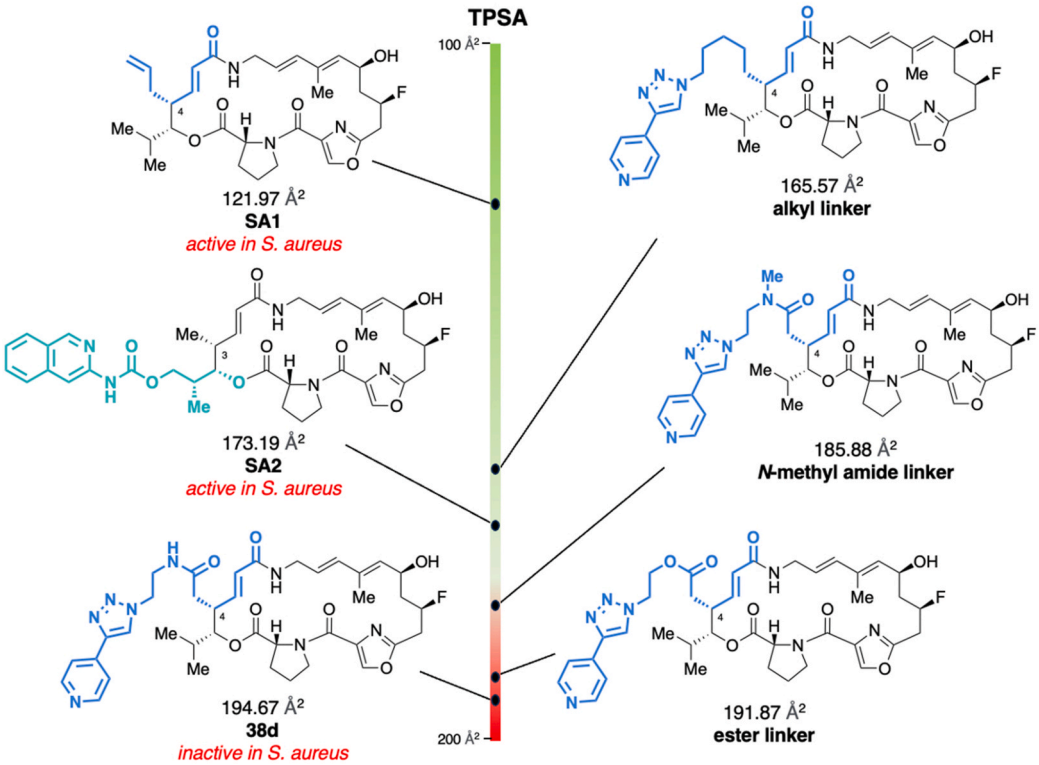

Fig. 4. Calculated TPSA ($Å^2$) of **SA1**, **SA2**, **38d**, and amide bioisosteres.

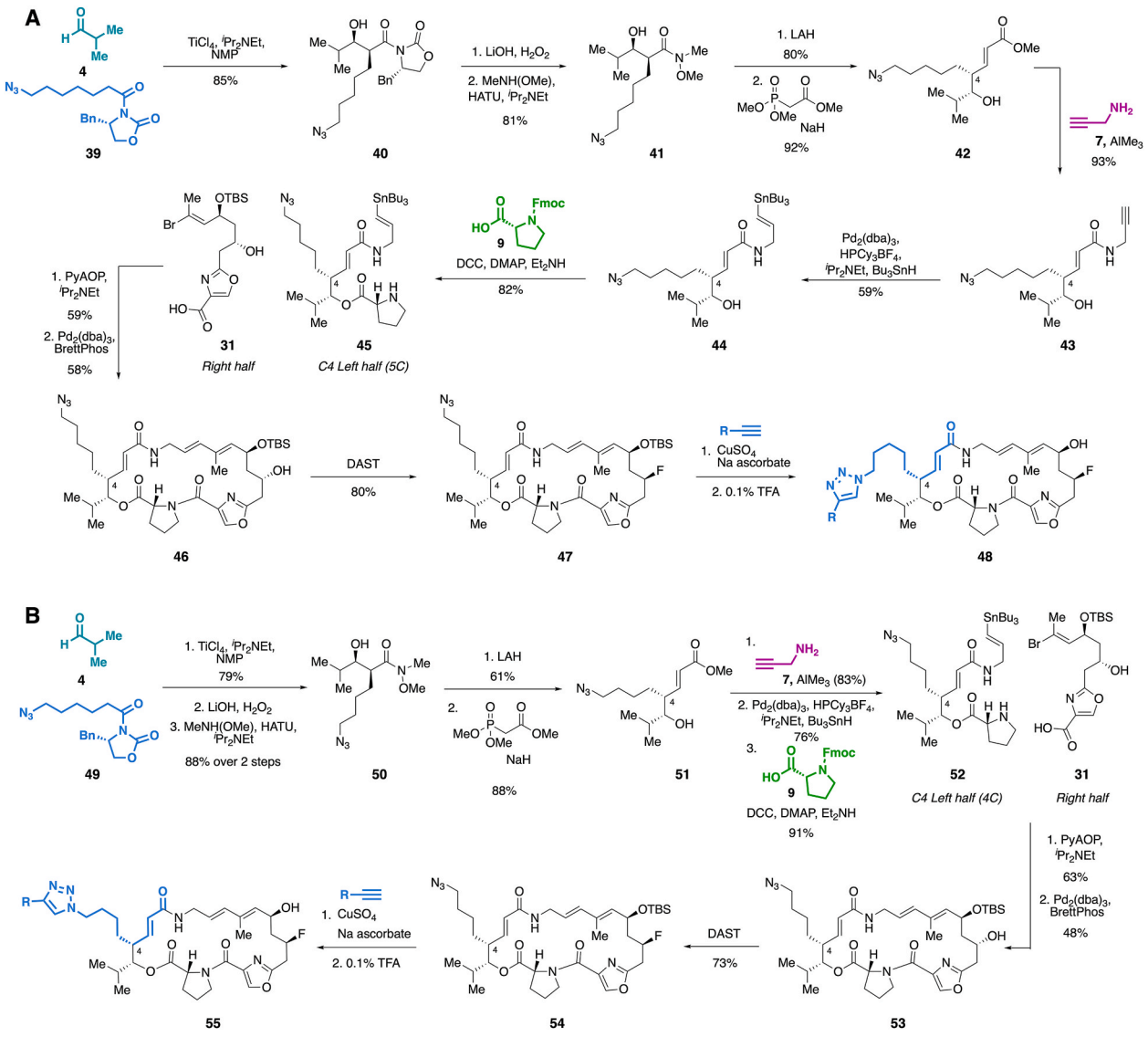

Scheme 4. A. Synthesis of 5-carbon linker analogs, with access to novel analogs **48**. **B.** Synthesis of 4-carbon linker analogs, with access to novel analogs **55**. Bu = butyl, Cy = cyclohexyl, dba = dibenzylideneacetone, DCC = dicyclohexylcarbodiimide, DMAP = 4-dimethylaminopyridine, Fmoc = 9-fluorenylmethoxycarbonyl, NMP = *N*-methyl-2-pyrrolidone, PyAOP = (7-azabenzotriazol-1-yloxy)tripyrrolidinophosphonium hexafluorophosphate, TBS = *tert*-butyldimethylsilyl.

We subjected azides **47** and **54** to click chemistry conditions in the presence of various aryl alkynes to deliver a library of C4-alkyl-aryl analogs, resulting in 17 novel streptogramin analogs bearing aryl-triazole sidechains (15 with five-carbon linkers, 2 with four-carbon linkers). Compared to the amide linker series, the alkyl linker series also incorporated more hydrophobic aryl substituents to reduce overall polarity. Additionally, structural diversity at various positions of the aryl ring was introduced to assess the effects of aryl substitution on activity (Fig. 5A).

2.4. Antibacterial efficacy

We evaluated the antibacterial activity of 17 C4-alkyl-aryl group A streptogramin analogs, the natural products **VM2** and **VS1**, the semi-synthetic group A streptogramin flopristin (**1**), and the combination of flopristin (**1**) with **VS1** against a panel of 18 pathogens (See Fig. 5A, SI Figure S4). These alkyl linker analogs showed an overall improvement in activity compared to the amide linker series (See Figs. 3A and 5B, SI Figures S2, S3 and S4). Replacing the polar amide group with a full carbon chain restored antibacterial activity, supporting our hypothesis that reducing TPSA can improve cellular permeability and efficacy.

Although none of the alkyl linker series surpassed activity of the combination of flopristin (**1**) with **VS1**, they exhibited greater potency than the naturally occurring streptogramins **VM2** and **VS1** independently (Fig. 5B and SI Figure S4). The 5-carbon linker series **48** demonstrated enhanced activity compared to the 4-carbon linker series **55**. This trend is evident when comparing the 5-carbon linker **48a** (4-pyridyl) to its 4-carbon linker counterpart **55a** (4-pyridyl), with the longer alkyl chain having better activity due to increased lipophilicity. In contrast, the 5-carbon linker **48b** (phenyl) and 4-carbon linker **55b** (phenyl) exhibited comparable activity, likely due to the lower polarity of the phenyl substituent compared to the 4-pyridyl group, which minimizes lipophilicity differences across linker lengths.

Within the 5-carbon series, subtle modifications to the aryl ring led to significant changes in activity. For instance, analogs **48a** (4-pyridyl) and **48k** (2-pyridyl) showed better activity than **48o** (3-pyridyl). The position of the pyridine nitrogen may influence the electronic character and orientation of the aryl ring in the binding pocket, affecting its ability to engage in productive π-stacking. Since the aryl rings are proposed to engage in π-stacking interactions with U1782, the 2- and 4-pyridyl analogs may adopt a more favorable stacking geometry compared to the 3-pyridyl analog. Additionally, **48c** (*p*-tolyl) and **48h** (*m*-tolyl) showed

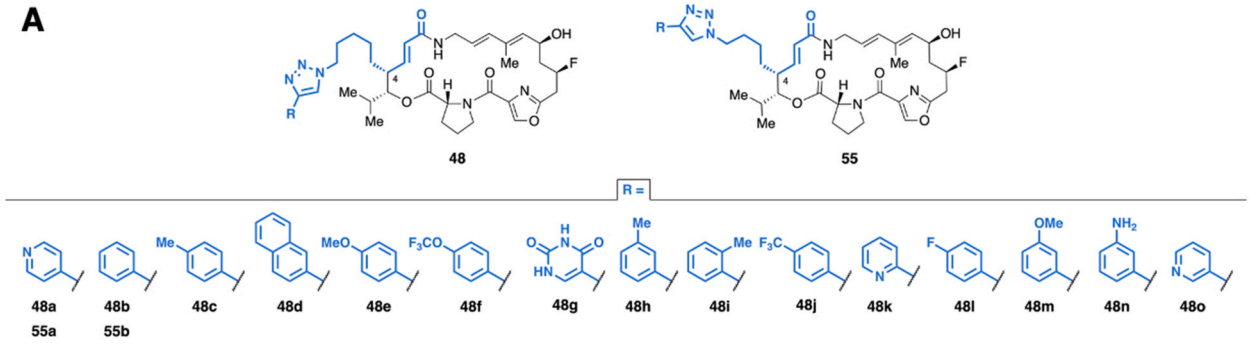

B

Minimal Inhibitory Concentration (MIC) Values (μg/mL)

strain:	*E. faecium* ATCC 35667	*E. faecium* VREfm (vanA) MMX 0752	*S. aureus* CLSI QC ATCC 29213	*S. aureus* Streptogramin A and B resistance (VatA, Vgb) MMX 10227	*S. aureus* MLSb ErmA resistance; inducible MMX 2321	*S. aureus* MLSb ErmA resistance; constitutive MMX 3035	*S. aureus* MLSb ErmC resistance MMX 3037	*S. aureus* MRSA USA 300	*S. pneumoniae* PSSP; CLS QC ATCC 49619	*S. pneumoniae* mef(A) MMX 3032	*S. pneumoniae* erm(B) MMX 3033
Compound ID											
VM2	2	16	16	64	16	8	4	16	16	8	64
flopristin	0.25	1	0.5	8	0.5	0.5	0.25	0.5	1	0.5	2
VS1	8	32	32	>64	32	>64	>64	16	4	4	32
flopristin + VS1	≤0.06	0.12	≤0.06	1	≤0.06	0.12	≤0.06	≤0.06	≤0.06	0.12	≤0.06
48a	2	8	2	8	4	4	1	4	1	1	4
48b	2	8	2	4	4	4	1	4	4	4	16
48c	1	4	4	4	4	2	0.5	2	4	2	8
48d	>64	>64	>64	>64	>64	>64	2	>64	>64	32	>64
48e	4	16	8	16	8	8	2	8	8	8	32
48f	>64	>64	>64	>64	>64	>64	2	>64	>64	>64	>64
48g	16	8	32	64	64	32	8	32	1	1	8
48h	2	>64	4	4	4	2	1	4	4	2	16
48i	>64	>64	>64	>64	>64	>64	>64	>64	>64	>64	>64
48j	4	16	>64	>64	>64	>64	2	>64	>64	>64	>64
48k	2	16	8	8	8	4	1	4	4	2	16
48l	2	16	8	8	4	4	0.5	4	8	4	16
48m	4	>64	8	8	8	4	1	4	4	4	16
48n	4	>64	8	16	8	4	1	8	4	4	16
48o	8	>64	32	64	16	16	4	16	8	8	32
55a	2	32	8	32	16	8	4	8	2	2	8
55b	1	8	2	4	4	2	1	2	2	2	8

Fig. 5. A. Library of C4-modified alkyl linker analogs **48** and **55**. **B.** MIC values (μg mL^{-1}) for selected analogs against an expanded panel of pathogens. Each MIC was obtained in technical triplicate. MLSb = macrolide, lincosamide, streptogramin B.

excellent activity, whereas **48i** (*o*-tolyl) completely lost activity, suggesting that para and meta substitutions were better tolerated than ortho substitutions. The diminished activity of **48i** may be due to intramolecular steric interactions between the ortho substituent and the triazole, distorting ring orientation and compromising π-stacking interactions with U1782-U2586. Similarly, certain substituents at the para position – such as the naphthyl group in **48d**, -OCF_3 in **48f**, and -CF_3 in **48j** – led to significantly reduced activity across multiple strains, possibly due to steric clashes with U2609 in the binding pocket (Fig. 3C). Interestingly, the polar uracil ring in **48g** had the potential to pick up an additional interaction with U2609 (Fig. 3C), but this was not borne out in its cellular activity. The increased polarity from the uracil ring may be reducing permeability and cellular entry, thereby diminishing its overall activity.

The most potent analogs – **48a**, **48c**, and **55b** – demonstrated superior activity compared to **VM2** against multiple bacterial strains. These analogs retained activity against strains resistant to both group A and group B streptogramins, including a 8- to 16-fold increase in potency against VatA/Vgb *S. aureus* relative to **VM2** (64 vs 4-8 μg mL^{-1}) and **VS1** (>64 vs 4-8 μg mL^{-1}) as well as a 64- to 128-fold increase in potency against ErmC *S. aureus* relative to **VS1** (>64 vs 0.5-1 μg mL^{-1}). Analogs **48c** and **55b** also had a 2-fold increase in potency against VatA/Vgb *S. aureus* relative to flopristin (**1**) (8 vs 4 μg mL^{-1}). These results highlight the ability of these group A streptogramins, with extensions that reach into the group B binding site, in overcoming resistance mechanisms that target both group A and group B streptogramins.

To elucidate the structural basis of antibacterial activity, we determined a cryo-EM structure based on a 2.5-Å reconstruction of **48a** bound to the *E. coli* ribosome (Fig. 6A, PDB code 10QM). The alkyl linker analog **48a** closely overlaid the amide linker analog **38d**, preserving the π-stacking interactions between the triazole–pyridyl moiety and U1782–U2586. In addition, the alkyl linker of **48a** engaged in an additional van der Waals interaction with U2585 that was not observed for the amide linker of **38d** (Fig. 6B). These additional contacts, together with improved permeability, may contribute to the enhanced activity of **48a**. Notably, the C4 sidechain of **48a** occupied the same binding site as tetracenomycin X, enabling the anticipated π-stacking interaction with the U1782–U2586 base pair (Fig. 6C). Furthermore, overlay of **48a** with **VS1** revealed that the aryltriazole sidechain mimicked multiple van der Waals interactions formed by **VS1** within the binding site (Fig. 6D).

While the alkyl linker series addressed limitations in cellular activity, additional optimization will be required to achieve a highly potent group A streptogramin with C4 derivatization. We speculate that the conformational flexibility of the alkyl linker may be increasing the

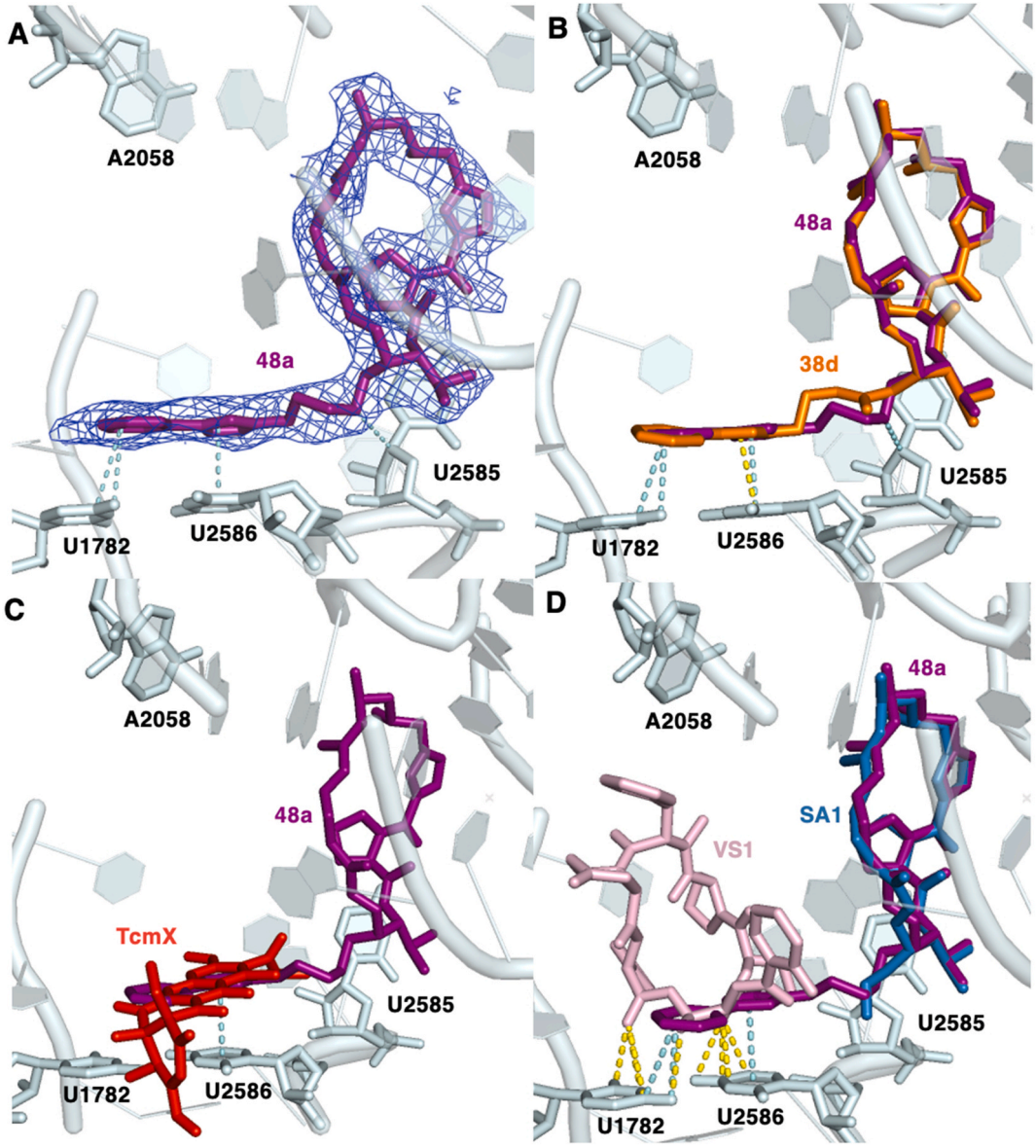

Fig. 6. A. Cryo-EM structure based on a 2.5-Å resolution Coulomb potential density map for ribosomes bound to **48a**. **48a** is making van der Waals (VDW) interactions (blue dashed lines) with U1782-U2586 and U2585. **B.** Overlay of cryo-EM structures of ribosome-bound **48a** (purple, PDB code 10QM) and **38d** (orange, PDB code 8E36) reveals π-stacking interaction with U2586 in **38d** (yellow dashed line) is maintained in **48a** (blue dashed line). **C.** Overlay of cryo-EM structures of ribosome-bound **48a** (purple) and **TcmX** (red, PDB code 6Y69). **D.** Overlay of cryo-EM structures of ribosome-bound **48a** (purple) with **SA1** (blue) and **VS1** (pink, PDB code 6WYV) reveals the C4 sidechain mimicking a few VDW interactions (blue dashed lines) that **VS1** makes (yellow dashed lines).

entropic penalty of binding, and future iterations could benefit from rigidification of the linker. The extension tolerated variation in ring size and substitution patterns, suggesting that additional C4 modifications, including meta-substituted aryl rings or compact 5-membered aromatic rings, may further enhance binding. Ongoing structure-guided optimization, informed by cryo-EM, will be used to identify a highly active group A streptogramin capable of potent antibacterial activity without the need for group B synergy.

3. Conclusion

Through an integrated approach combining structure-based drug design, modular chemical synthesis, antibacterial evaluation, and high-resolution cryo-EM, we developed a new class of group A streptogramins. Incorporation of aryltriazole-bearing sidechains at the C4 position resulted in additional contacts within the ribosome exit tunnel. Early designs utilized an amide-containing linker to incorporate the sidechain and had poor antibacterial activity. Utilizing TPSA to redesign analogs with improved permeability, replacement of the amide linker with a nonpolar alkyl linker led to greatly improved activity. Several analogs of the alkyl linker series demonstrated efficacy against resistant strains, including *S. aureus* with VatA and VgB resistance. This proof-of-concept establishes a design framework for developing group A streptogramins as potent monotherapies. Continued design, optimization, and synthesis of group A streptogramins will expand the utility of the streptogramin class and contribute to the antibiotic pipeline.

CRediT authorship contribution statement

Isabel J. Lee: Conceptualization, Data curation, Formal analysis, Investigation, Methodology, Validation, Visualization, Writing – original draft, Writing – review & editing. **Qi Li:** Conceptualization, Data curation, Formal analysis, Investigation, Methodology, Writing – review & editing. **Tushar Raskar:** Data curation, Formal analysis,

Investigation, Methodology, Visualization, Writing – review & editing. **Jenna Pellegrino:** Data curation, Formal analysis, Investigation, Methodology, Visualization, Writing – review & editing. **Andrew K. Ecker:** Data curation, Formal analysis, Investigation, Methodology, Writing – review & editing. **Sara Y. Howard:** Investigation, Methodology. **James S. Fraser:** Conceptualization, Data curation, Formal analysis, Funding acquisition, Project administration, Resources, Supervision, Writing – review & editing. **Ian B. Seiple:** Conceptualization, Data curation, Formal analysis, Funding acquisition, Project administration, Resources, Supervision, Visualization, Writing – original draft, Writing – review & editing.

Declaration of competing interest

The authors declare the following financial interests/personal relationships which may be considered as potential competing interests: Ian B. Seiple reports financial support was provided by National Institute of General Medical Sciences. James S. Fraser reports financial support was provided by National Institute of General Medical Sciences. James S. Fraser reports a relationship with Interdict Bio that includes: board membership. James S. Fraser reports a relationship with Relay Therapeutics Inc. that includes: consulting or advisory and funding grants. If there are other authors, they declare that they have no known competing financial interests or personal relationships that could have appeared to influence the work reported in this paper.

Acknowledgements

This work is supported by NIH GM148184. J.S.F is supported by NIH GM145238. Cryo-EM equipment at UCSF is partially supported by NIH grants S10OD020054, S10OD021741 and S10OD026881 and Howard Hughes Medical Institute. We thank A. Mendez and D. Hufnagel at Microbiologics for conducting the expanded MIC assays against both Gram-positive and Gram-negative bacteria including those with specific resistance mechanisms. We thank Z. Zhou at the QB3/Chemistry Mass Spectrometry Facility at University of California, Berkeley for collecting high-resolution mass spectra of our compounds. We thank the Bachrach Family Foundation for their generous support to our antibiotic program.

Appendix A. Supplementary data

Supplementary data to this article can be found online at https://doi.org/10.1016/j.ejmech.2026.118947.

Data availability

Cryo-EM table contains information on cryo-EM structures and deposition numbers. All other data can be found in the Supporting Information file.

References

[1] S. Reissier, V. Cattoir, Streptogramins for the treatment of infections caused by gram-positive pathogens, Expert Rev. Anti Infect. Ther. 19 (5) (2021) 587–599.
[2] R. Khosla, D.D. Verma, A. Kapur, R.V. Aruna, N. Khanna, Streptogramins: a new class of antibiotics, Indian J. Med. Sci. 53 (3) (1999) 111–119.
[3] C. Gurk-Turner, Quinupristin/dalfopristin: the first available macrolide-lincosamide-streptogramin antibiotic, SAVE Proc. 13 (1) (2000) 83–86.
[4] J.R. Aeschlimann, M.J. Zervos, M.J. Rybak, Treatment of vancomycin-resistant Enterococcus faecium with RP 59500 (Quinupristin-Dalfopristin) administered by intermittent or continuous infusion, alone or in combination with doxycycline, in an in vitro pharmacodynamic infection model with simulated endocardial vegetations, Antimicrob. Agents Chemother. 42 (10) (1998) 2710–2717.
[5] Synercid® I.V. (quinupristin and dalfopristin for injection). https://www.accessdata.fda.gov/drugsatfda_docs/label/2017/050747s015,050748s014lbl.pdf.
[6] L.E. López-Jacome, Y.M. Mercado-Casillas, B.J. Méndez-Sotelo, J.G. Jiménez-Cortes, A. Tovar-García, A.Y. Estrada-Velasco, J.A. Almeida-Villegas, J.D. P. Martínez, R. García-Contreras, Anti-bacterial agents, in: Encyclopedia of Infection and Immunity, Elsevier, 2022, pp. 494–509.
[7] J. Noeske, J. Huang, N.B. Olivier, R.A. Giacobbe, M. Zambrowski, J.H.D. Cate, Synergy of streptogramin antibiotics occurs independently of their effects on translation, Antimicrob. Agents Chemother. 58 (9) (2014) 5269–5279.
[8] P.J. Stogios, M.L. Kuhn, E. Evdokimova, P. Courvalin, W.F. Anderson, A. Savchenko, Potential for reduction of streptogramin A resistance revealed by structural analysis of acetyltransferase VatA, Antimicrob. Agents Chemother. 58 (12) (2014) 7083–7092.
[9] Q. Li, J. Pellegrino, D.J. Lee, A.A. Tran, H.A. Chaires, R. Wang, J.E. Park, K. Ji, D. Chow, N. Zhang, A.F. Brilot, J.T. Biel, G. van Zundert, K. Borrelli, D. Shinabarger, C. Wolfe, B. Murray, M.P. Jacobson, E. Mühle, O. Chesneau, J. S. Fraser, I.B. Seiple, Synthetic group A streptogramin antibiotics that overcome vat resistance, Nature 586 (7827) (2020) 145–150.
[10] I.A. Osterman, M. Wieland, T.P. Maviza, K.A. Lashkevich, D.A. Lukianov, E. S. Komarova, Y.V. Zakalyukina, R. Buschauer, D.I. Shiriaev, S.A. Leyn, J.E. Zlamal, M.V. Biryukov, D.A. Skvortsov, V.N. Tashlitsky, V.I. Polshakov, J. Cheng, Y. S. Polikanov, A.A. Bogdanov, A.L. Osterman, S.E. Dmitriev, R. Beckmann, O. A. Dontsova, D.N. Wilson, P.V. Sergiev, Tetracenomycin X inhibits translation by binding within the ribosomal exit tunnel, Nat. Chem. Biol. 16 (10) (2020) 1071–1077.
[11] G.G. Zhanel, E. Hartel, H. Adam, S. Zelenitsky, M.A. Zhanel, A. Golden, F. Schweizer, B. Gorityala, P.R.S. Lagacé-Wiens, A.J. Walkty, A.S. Gin, D.J. Hoban, J.P. Lynch, J.A. Karlowsky, Solithromycin: a novel fluoroketolide for the treatment of community-acquired bacterial pneumonia, Drugs 76 (18) (2016) 1737–1757.
[12] I.B. Seiple, Z. Zhang, P. Jakubec, A. Langlois-Mercier, P.M. Wright, D.T. Hog, K. Yabu, S.R. Allu, T. Fukuzaki, P.N. Carlsen, Y. Kitamura, X. Zhou, M.L. Condakes, F.T. Szczypiński, W.D. Green, A.G. Myers, A platform for the discovery of new macrolide antibiotics, Nature 533 (7603) (2016) 338–345.
[13] J. Pellegrino, D.J. Lee, J.S. Fraser, I.B. Seiple, E. coli 50S ribosome bound to solithromycin and VM1. Worldwide Protein Data Bank, Worldwide Protein Data Bank, 2022, https://doi.org/10.2210/pdb8e3o/pdb.
[14] J.-L. Pernodet, S. Fish, M.-H. Blondelet-Rouault, E. Cundliffe, The macrolide-lincosamide-streptogramin B resistance phenotypes characterized by using a specifically deleted, antibiotic-sensitive strain of streptomyces lividans, A NTIMICROBIAL A GENTS AND C HEMOTHERAPY 40 (3) (1996) 581–585.
[15] T.A. Mukhtar, K.P. Koteva, D.W. Hughes, G.D. Wright, Vgb from Staphylococcus Aureus inactivates streptogramin B antibiotics by an elimination mechanism not hydrolysis, Biochemistry 40 (30) (2001) 8877–8886.
[16] Q. Li, I. B. Modular Seiple, Scalable synthesis of group A streptogramin antibiotics, J. Am. Chem. Soc. 139 (38) (2017) 13304–13307.
[17] Q. Li, I.B. Seiple, A concise route to virginiamycin M2, Tetrahedron 75 (24) (2019) 3309–3318.
[18] Q. Li, I.B. Seiple, Modular synthesis of streptogramin antibiotics, Synlett 32 (7) (2021) 647–654.
[19] D.A. Evans, J.M. Takacs, L.R. McGee, M.D. Ennis, D.J. Mathre, J. Bartroli, Chiral enolate design, Pure Appl. Chem. 53 (6) (1981) 1109–1127.
[20] Horner-Wadsworth-Emmons Olefination. *Comprehensive Organic Name Reactions and Reagents*, John Wiley & Sons, Inc., Hoboken, NJ, USA, 2010, pp. 1484–1490, https://doi.org/10.1002/9780470638859.conrr332.
[21] M.T. Crimmins, K. Chaudhary, Titanium enolates of thiazolidinethione chiral auxiliaries: versatile tools for asymmetric aldol additions, Org. Lett. 2 (6) (2000) 775–777.
[22] D. Romo, N.S. Choi, S. Li, I. Buchler, Z. Shi, J.O. Liu, Evidence for separate binding and scaffolding domains in the immunosuppressive and antitumor marine natural product, pateamine a: design, synthesis, and activity studies leading to a potent simplified derivative, J. Am. Chem. Soc. 126 (34) (2004) 10582–10588.
[23] D.A. Entwistle, Total synthesis of oxazole-based virginiamycin antibiotics: 14,15-Anhydropristinamycin IIB, Synthesis (Mass.) 1998 (S1) (1998) 603–612.
[24] E.J. Corey, M.G. Bock, A.P. Kozikowski, A.V.R. Rao, D. Floyd, B. Lipshutz, A key intermediate for the synthesis of maytansine and related antitumor agents, Tetrahedron Lett. 19 (12) (1978) 1051–1054.
[25] A.J. Phillips, Y. Uto, P. Wipf, M.J. Reno, D.R. Williams, Synthesis of functionalized oxazolines and oxazoles with DAST and deoxo-fluor, Org. Lett. 2 (8) (2000) 1165–1168.
[26] J.R. Parikh, W.v.E. Doering, Sulfur trioxide in the oxidation of alcohols by dimethyl sulfoxide, J. Am. Chem. Soc. 89 (21) (1967) 5505–5507.
[27] G.A. Kraus, B. Roth, Synthetic studies toward verrucarol. 2. Synthesis of the AB ring system, J. Org. Chem. 45 (24) (1980) 4825–4830.
[28] A. Raach, O. Reiser, Sodium chlorite-hydrogen peroxide — a mild and selective reagent for the oxidation of aldehydes to carboxylic acids, J. Prakt. Chem. 342 (6) (2000) 605–608.
[29] V.V. Rostovtsev, L.G. Green, V.V. Fokin, K.B.A. Sharpless, Stepwise huisgen cycloaddition process: copper(i)-catalyzed regioselective "Ligation" of azides and terminal alkynes, Angew. Chem. Int. Ed Engl. 41 (14) (2002) 2596–2599.
[30] J. Pellegrino, D.J. Lee, J.S. Fraser, I.B. Seiple, E. coli 50S ribosome bound to compound streptogramin A analog 3146, Worldwide Protein Data Bank 28 (6) (2023), https://doi.org/10.2210/pdb8e36/pdb.
[31] J. Pellegrino, D.J. Lee, J.S. Fraser, I.B. Seiple, E. coli 50S ribosome bound to compound streptogramin A analog 3142, Worldwide Protein Data Bank, Worldwide Protein Data Bank, , 2022, https://doi.org/10.2210/pdb8e30/pdb.
[32] N.K. Boyd, C. Teng, C.R. Frei, Brief overview of approaches and challenges in new antibiotic development: a focus on drug repurposing, Front. Cell. Infect. Microbiol. 11 (2021) 684515.
[33] C.A. Lipinski, F. Lombardo, B.W. Dominy, P.J. Feeney, Experimental and computational approaches to estimate solubility and permeability in drug discovery and development settings, Adv. Drug Deliv. Rev. 46 (1–3) (2001) 3–26.

[34] A. Gaurav, P. Bakht, M. Saini, S. Pandey, R. Pathania, Role of bacterial efflux pumps in antibiotic resistance, virulence, and strategies to discover novel efflux pump inhibitors, Microbiology 169 (5) (2023) 001333.
[35] D. Gurvic, U. Zachariae, Multidrug efflux in gram-negative bacteria: structural modifications in active compounds leading to efflux pump avoidance, NPJ Antimicrob. Resist. 2 (1) (2024) 6.
[36] R. Richter, M.A.M. Kamal, M.A. García-Rivera, J. Kaspar, M. Junk, W.A.M. Elgaher, S.K. Srikakulam, A. Gress, A. Beckmann, A. Grißmer, C. Meier, M. Vielhaber, O. Kalinina, A.K.H. Hirsch, R.W. Hartmann, M. Brönstrup, N. Schneider-Daum, C.-M. Lehr, A hydrogel-based in vitro assay for the fast prediction of antibiotic accumulation in gram-negative bacteria, Mater. Today Bio 8 (100084) (2020) 100084.
[37] S. Prasanna, R.J. Doerksen, Topological polar surface area: a useful descriptor in 2D-QSAR, Curr. Med. Chem. 16 (1) (2009) 21–41.
[38] L. David, M. Wenlock, P. Barton, A. Ritzén, Prediction of chameleonic efficiency, ChemMedChem 16 (17) (2021) 2669–2685.
[39] A.K. Ecker, D.A. Levorse, D.A. Victor, M.J. Mitcheltree, Bioisostere effects on the EPSA of common permeability-limiting groups, ACS Med. Chem. Lett. 13 (6) (2022) 964–971.
[40] G.H. Goetz, L. Philippe, M.J. Shapiro, EPSA: a novel supercritical fluid chromatography technique enabling the design of permeable cyclic peptides, ACS Med. Chem. Lett. 5 (10) (2014) 1167–1172.
[41] M.T. Crimmins, J. She, An improved procedure for asymmetric aldol additions WithN-Acyl oxazolidinones, oxazolidinethiones and thiazolidinethiones, Synlett (8) (2004) 1371–1374.
[42] A. Darwish, A. Lang, T. Kim, J.M. Chong, The use of phosphine ligands to control the regiochemistry of Pd-Catalyzed hydrostannations of 1-Alkynes: synthesis of (E)-1-Tributylstannyl-1-Alkenes, Org. Lett. 10 (5) (2008) 861–864.
[43] J.C. Cochran, S.C. Bayer, J.T. Bilbo, M.S. Brown, L.B. Colen, F.J. Gaspirini, D. W. Goldsmith, M.D. Jamin, K.A. Nealy, Kinetics of the protodestannylation of vinyltrialkyltins and substituted vinyltrialkyltins, Organometallics 1 (4) (1982) 586–590.
[44] D. Seyferth, Vinyl derivatives of the metals. II. The cleavage of vinyltin compounds by the halogens and by protonic Acids[1], J. Am. Chem. Soc. 79 (9) (1957) 2133–2136.
[45] L. Cai, I.B. Seiple, Q. Li, Modular chemical synthesis of streptogramin and lankacidin antibiotics, Acc. Chem. Res. 54 (8) (2021) 1891–1908.